Development of a radio-frequency ion beam source for fast-ion studies on the large plasma device

S. K. P. Tripathi, P. Pribyl, and W. Gekelman
Physics and Astronomy, University of California at Los Angeles, Los Angeles, California 90095, USA

(Received 4 June 2011; accepted 10 August 2011; published online 1 September 2011)

A helium ion beam source (23 kV/2.0 A) has been constructed for studying fast-ion physics in the cylindrical magnetized plasma of the large plasma device (LAPD). An inductive RF source produces a 10^{19} m^{-3} density plasma in a ceramic dome. A multi-aperture, rectangular (8 cm × 8 cm) three-grid system extracts the ion beam from the RF plasma. The ion beam is injected at a variety of pitch angles with Alfvénic speeds in the LAPD. The beam current is intense enough to excite magnetic perturbations in the ambient plasma. Measurements of the ion beam profile were made to achieve an optimum beam performance and a reliable source operation was demonstrated on the LAPD. © *2011 American Institute of Physics*. [doi:10.1063/1.3631628]

I. INTRODUCTION

Ion beam sources have widespread applications in industrial plasmas,[1,2] neutral-beam injection (NBI) systems for fusion devices,[3–5] bio-medical sciences,[6] particle accelerators,[7] and mass-spectrometry.[8] The terms "ion beam source" and "ion source" are used interchangeably in the science literature. The design criteria for ion sources differ from one application to another depending on the specific requirements of the application. Development of an ion source for fusion-relevant fast-ion studies on the large plasma device (LAPD) (Ref. 9) has been described in this article. The LAPD ion source injects a He ion beam (not a neutral beam) in either the main or afterglow plasma of the LAPD.

The large plasma device produces a quiescent, cylindrical, magnetized plasma with ~18 m maximum length, 0.75 m diameter, 10–20 ms pulse width τ_w, and 1.0 Hz repetition-rate τ_r using a barium oxide coated hot cathode.[10] The LAPD operates round-the-clock and its plasma is routinely diagnosed in three-dimensions using computer-controlled movable probes. One of the unique features of the LAPD plasma is its capability to accommodate traveling modes of shear Alfvén waves that ubiquitously exist in laboratory, space, and fusion plasmas. Shear Alfvén waves are transverse low frequency waves ($f < f_{ci}$) in magnetized plasmas that primarily propagate along the magnetic field.[11,12] The Alfvén speed is given by

$$v_A = \frac{B}{\sqrt{\mu_0 n_i m_i}}, \quad (1)$$

where, B is the magnetic field strength, n_i is the plasma density, and m_i is the ion mass. The parallel phase velocity of a shear Alfvén wave generated by an exciter with a large cross-field length-scale $L_\perp$ is nearly equal to v_A. A more general dispersion relation for shear Alfvén waves indicate oblique propagation of phase fronts forming a cone when $L_\perp \lesssim$ electron skin depth c/ω_{pe} in the inertial regime ($v_A > v_e$) (Ref. 13) and $L_\perp \lesssim$ ion sound gyro-radius c_s/ω_{ci} in the kinetic regime ($v_A < v_e$).[14] Here, ω_{pe}, ω_{ci}, v_e, and c_s are angular electron plasma frequency, angular ion cyclotron frequency, electron thermal speed, and ion sound speed, respectively.

A fast ion, in our experiment, is an energetic ion that moves with a speed comparable to the Alfvén speed in a magnetized plasma. In a fusion-grade Tokamak plasma, main sources of the fast-ions are alpha particles (doubly ionized helium nuclei) and energetic-ions generated by the radio frequency (RF) and NBI systems. Such fast-ions are observed to carry significant energy, excite energetic particle, and Alfvén wave modes, and directly affect the stability and energy confinement of the plasma.[15,16] Therefore, a basic understanding of the fast-ion physics is vital for improving the performance of the magnetically confined fusion plasmas. Although, several experiments related to fast-ions have been performed on Tokamaks,[16] the challenging task of diagnosing a hot plasma core ($T_e \gg 1$ keV) and complications arising due to the curvature effects of the Tokamak, warrant a controlled study of the basic physics of the fast-ions in a linear device where plasma can be easily diagnosed. The LAPD provides an ideal platform for such fast-ion studies.

II. DESIGN GOALS FOR THE LAPD ION SOURCE

The main equipment for performing the fast-ion studies on the LAPD is a He ion beam source that is discussed in this paper. The nature of the fast-ion interaction critically depends on the ion beam speed relative to the Alfvén speed[16] and it is important that both the sub-Alfvénic and super-Alfvénic regimes of the ion beam propagation are investigated. Typical Alfvén speed in a helium plasma of the LAPD is 7.7 × 10^5 m/s ($n_i = 2 \times 10^{18}$ m^{-3}, B = 0.1 T) which corresponds to 12.4 keV ion beam energy [$E_b = 0.5\, m_b v_b^2/e$]. Here, e is the elementary charge, m_b is the ion mass in the beam, v_b is the beam speed, and E_b is the beam energy in eV. Although, the Alfvén speed in the LAPD can be varied to the some extent by changing the plasma parameters, a 20 keV ion beam energy ($v_b = 9.8 \times 10^5$ m/s) was targeted for the ion source to provide us flexibility in accessing the super-Alfvénic regime of the beam propagation.

The requirement on the beam intensity comes from the fact that the fast-ion population in the LAPD plasma should be sufficient to destabilize Alfvén and energetic

particle modes.[15] The beam $\beta_b = 2\mu_0 e n_b E_b / B^2$ (ratio of the beam pressure and magnetic pressure) and plasma $\beta_p = 2\mu_0 e n_i T_e / B^2$ (ratio of the plasma pressure and magnetic pressure) are used in the growth rate calculations for fast-ion instabilities.[16,17] The LAPD fast-ion experiment has a design goal to achieve $\beta_b/\beta_p > 1$ using an ion beam with a 8.0 cm × 8.0 cm rectangular cross-sectional area ($A_b = 64$ cm^2). This implies that the required beam density ($n_b > n_i T_e / E_b$) for a 20 keV helium ion beam in the main LAPD plasma ($T_e \sim 5.0$ eV) is 5.0×10^{14} m^{-3}. Thus, the required beam current ($I = n_b e A v_b$) is ~ 0.5 A and the associated current density j_b is 7.8 mA/cm^2. In the afterglow of the LAPD plasma, the β_p monotonically drops to an order of magnitude lower value and much higher β_b/β_p can be achieved there. The 20 kV/0.5 A ion source has been constructed to satisfy following additional features:

1. The source provides flexibility in the beam injection at a variety of pitch angles into the LAPD.
2. An average gas pressure in the beam path is kept below 10^{-2} Pa (1 Pa = 7.5×10^{-3} Torr = 10^{-2} mbar) to minimize the charge exchange loss of the ion beam.
3. Necessary means for the space-charge neutralization and focusing of the ion beam have been developed to mitigate the beam blow-up.[7]
4. The source operates with a 0.25–1.0 Hz τ_r.
5. A reliable control system has been developed to facilitate an unattended and continuous operation of the ion source. This is critical for acquiring the high-resolution data on the LAPD.

The LAPD fast-ion experiment is the first of its kind where a super-Alfvénic ion beam is injected into a large cylindrical magnetized plasma. Hence, the LAPD ion source is built to fulfill several unique requirements as discussed above. Unlike NBI sources where the ultimate goal is to inject a neutral beam to heat a plasma, the LAPD ion source must produce an ion beam, with a low fraction of neutrals, for studying the waves (e.g., Cherenkov emission of an Alfvén wave) generated by the fast-ions in the LAPD plasma. The ion beam must travel through the diverging magnetic field at the end of the device to get into the main plasma and it must maintain a low beam divergence ($< 1.5^\circ$) while traversing a long path (~ 4.8 m) to minimize the beam losses.

We begin the remaining parts of this paper by presenting an elementary model of the ion beam extraction in Sec. III. This is followed by the description of the source assembly in Sec. IV which incorporates details of the plasma source, beam extractor, vacuum system, and control system. The experimental results are discussed in Sec. V.

III. ELEMENTARY MODEL FOR OPTIMUM BEAM EXTRACTION

The perveance P of a multi-aperture ion beam source is given by[18]

$$P = \frac{I}{{V_0}^{3/2}} = \frac{j\pi N D^2}{4{V_0}^{3/2}}, \tag{2}$$

where I is the beam current, V_0 is the beam extraction voltage, j is the average current density, N is the number of apertures, and D is the aperture diameter. The maximum current density j_{max} of an ideal ion source with planar grids is limited by the space-charge in accordance with the Child-Langmuir law,

$$j_{max} = \frac{4\epsilon_0}{9}\sqrt{\frac{2eZ}{M}}\frac{{V_0}^{3/2}}{d_1^2}, \tag{3}$$

where M is the ion mass, Z is its charge state, and d_1 is the accelerating gap. Divergence of a space charge limited ion-beam has been estimated by Coupland *et al.*,[19] Ray *et al.*,[20] and Kim *et al.*[18] (more references therein). It was analytically derived and experimentally demonstrated that a minimum beam divergence is achieved when $j \simeq j_{max}/2.14$. This condition implies that the optimum beam current density,

$$j_b = \frac{K}{2.14}\frac{V_0^{3/2}}{d_1^2}, \quad \text{where } K = \frac{4\epsilon_0}{9}\sqrt{\frac{2eZ}{M}}. \tag{4}$$

For a helium ion beam $K = 2.7 \times 10^{-8}$ A–V$^{-3/2}$. Derivation of the minimum beam divergence condition in the above equation does not include the effect of the beam blow up due to beam-plasma instabilities, collisions, or inadequate space-charge compensating electrons in the beam path. It also assumes that a stable and nearly spherical sheath boundary is established in the screen-grid aperture.

IV. ION SOURCE ASSEMBLY

The essential components of the ion source assembly are illustrated in Fig. 1. The assembly can be divided in three major parts: the plasma chamber, beam extractor, and ion source vacuum chamber. Details of these parts and the ion source control system are described in Secs. IV A–IV D.

A. RF plasma source

An RF source has been constructed for producing an inductively coupled plasma (ICP) (Ref. 21) for the ion source. The ICP is produced in a ceramic dome (inner diam: 0.53 m, plasma volume: 0.04 m^{-3}) using a twenty-eight turn water-cooled copper inductor wound on the external surface of the ceramic dome. The external winding of the coil is preferred over internal winding, since the maintenance of the ICP source with external coils does not require a vacuum break. It also saves a considerable time in conditioning the ion-source grids and keeps the plasma free from the electrode impurities. The external winding also provides flexibility in tuning the circuit elements and helps avoid a multitude of problems such as electrode erosion, water leaks from punctured tubes in the vacuum system, unipolar arcs by the near-fields of the internal antenna structures, and excessive heat load on the ion-source grids when hot-cathode type plasma sources are used.

The circuit diagram of the ICP source is displayed in Fig. 2. Four units of MOSFET based push-pull amplifiers are connected in a two-stage parallel configuration to deliver up to 28 kW of the pulsed RF power ($\tau_w = 2.0$ ms) to the plasma. The parallel connections of the amplifiers utilize a passive current-sharing scheme to protect them from damage due to

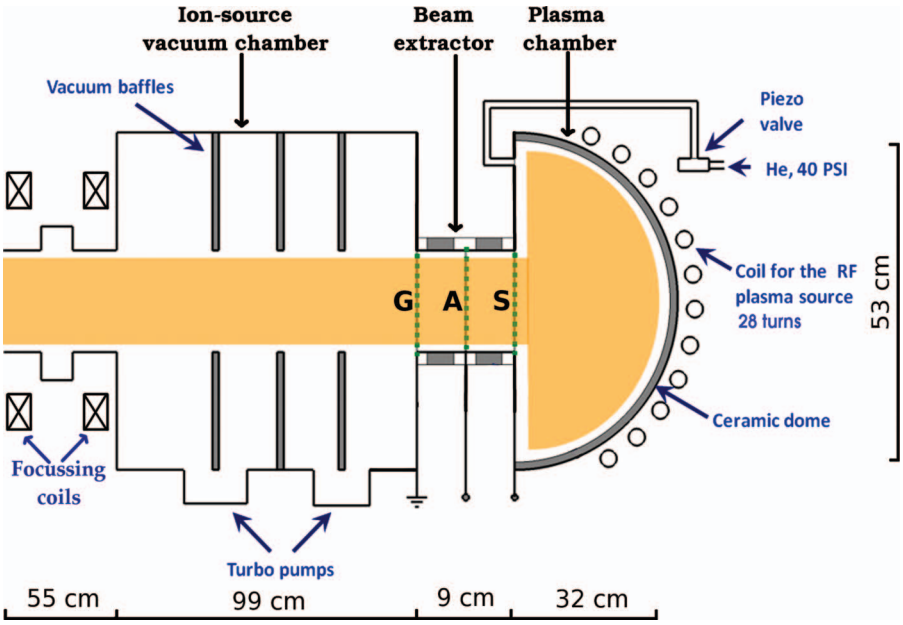

FIG. 1. (Color online) Schematic of the ion source showing the plasma chamber, beam extractor, and ion-source vacuum chamber. The left-side of the vacuum chamber has a flexible bellow (see Fig. 4) which connects to the LAPD to facilitate the beam injection at a variety of pitch angles.

any asymmetric-current loading. The RF source operates in the 0.3–0.6 MHz frequency range. The lower frequency, compared to 13.56 MHz and higher frequencies, is used for the following two reasons. First, a compact and economical RF source could be built in the lower frequency range using a simple switching transistor circuit. This circuit avoids use of a traditional matching network.[22] Second, the radiation from the circuit elements to the surroundings is less severe at lower frequencies which makes the design of the RF shielding and transmission lines much easier.

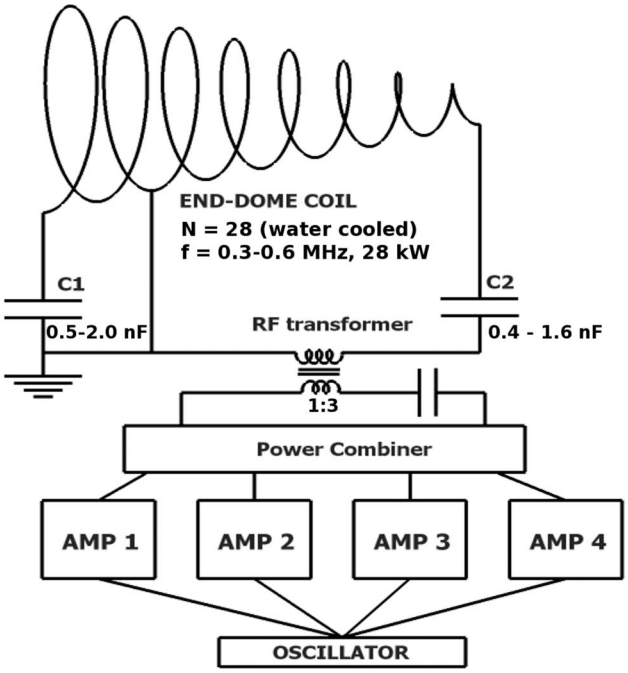

FIG. 2. Circuit diagram of the RF source. The end-dome coil delivers up to 28 kW RF power to the inductively coupled plasma in the end-dome.

The main disadvantage of using a RF plasma source is the presence of the RF oscillation in the beam current. In our setup, the beam current oscillation is generated by a capacitive coupling between the RF antenna and the metal support structure of the screen grid. This RF voltage appears across the screen-grid sheath and modulates the beam current. Note that even though a RF voltage appears across the screen-grid sheath, the plasma potential is not expected to have significant RF oscillations since the skin depth[23] ($\delta \sim c/\omega_{pe}$) for a $n > 10^{18}$ m^{-3} plasma is less than 5.3 mm and the plasma diameter is much larger. The beam current oscillation is minimized to less than 2% of the average beam current by adjusting the bypass capacitor C_1. The tuning capacitor C_2 is adjusted to obtain a resonant cavity response in the end dome which in turn provides a maximum efficiency in the plasma production. In certain beam-plasma experiments on the LAPD, it is desirable to modulate the beam below the ion cyclotron frequency to study the radiation pattern of the beam-current excited shear Alfvén waves. In such experiments, C_1 is detuned to maximize the RF oscillation across the screen-grid sheath.

A piezoelectric gas-flow valve (response time <2 ms, flow rate: 500 SCCM) injects helium neutral gas in the end dome ($\tau_w = 4.0$ ms). The gas-pulse raises the neutral pressure in the end-dome up to ~1 Pa. The RF source is turned on ~5.0 ms after the gas-valve trigger and an ICP is produced within 0.2 ms after the application of the RF voltage. The ion beam is extracted during the middle of the ICP pulse. This setup operates with a 0.25–1.0 Hz repetition rate. Timing of the gas-valve trigger is synchronized with the LAPD plasma to inject the beam at a desired time.

B. Beam extractor

The beam extractor consists of three multi-aperture molybdenum grids (thickness:1.0 mm), namely, the screen

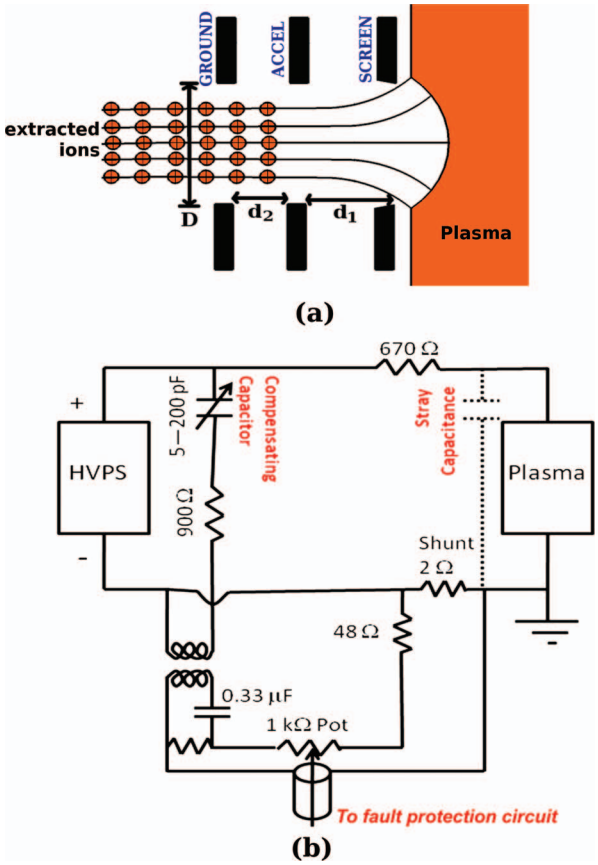

FIG. 3. (Color online) (a) Sketch of an ion beamlet extracted from the plasma by three apertures in the extraction grids. The LAPD ion beam has 1073 nearly identical ion beamlets. The beam exists to the left and moves toward the LAPD plasma. (b) A fast time response ($t < 2\ \mu$s) stray capacitance neutralization circuit for the arc-fault detection.

grid, accel grid, and ground grid. These grids are indicated by the letters S, A, and G in Fig. 1. Each one of the grids has 1073 apertures (diam:2 mm, transparency:57%) arranged in a 8 cm × 8 cm rectangular pattern. A close-up sketch of the apertures forming an ion beamlet from the plasma are shown in Fig. 3(a). In the existing setup, distance between the screen grid and accel grid, d_1, is 6.0 mm and distance between the accel and ground grid, d_2, is 1.3 mm. The apertures in the grids are carefully aligned to obtain a nearly unobstructed path for the ion beamlets. Performance characteristics of an ion beamlet formed from a single aperture three electrode system have been described by Coupland *et al.*[19] in detail.

Two tungsten filaments are placed in the ion beam path at 0.18 m and 0.74 m distances from the ground grid to provide necessary electrons for the space charge neutralization.[7] These filaments are turned on only when neutralizing electrons are needed in the stand-alone operation of the ion source and they are not used during the ion-source operation on the LAPD since the ambient LAPD plasma provides neutralizing electrons and prevents the beam blow-up.

A three-grid fast-ion collector[24,25] is used for measuring the ion beam profile. The fast-ion collector uses 200 lines per inch nickel grids with a ∼66% transparency. The bias voltage on the grids is adjusted to retard electrons and ions with less than 84 eV energy. The spatial resolution of the measured beam profile is limited by the size of the screen grid (diam: 5.0 mm) in the fast ion collector.

A high-voltage pulser ($V_{max} = 25$ kV, $\tau_w = 25\ \mu$s, −1.5 ms) provides the bias voltage V_s for the screen grid with respect to the ground grid. The 25 kV pulser has been built using very-high-voltage IGBTs ($V_{max} = 2.5$ kV, $I_{max} = 40$ A, rise time $< 0.25\ \mu$s). The accel grid is biased negative ($V_a = -0.05 V_s$) and the ground grid is held at the LAPD chamber potential.

C. Ion source vacuum chamber

A high density plasma ($n_{max} \sim 10^{19}$ m^{-3}) is produced by the RF source for extracting the ion beam. This requires up to 1 Pa neutral gas pressure in the plasma chamber. It is impractical to maintain continuously such a high neutral pressure in the ion source chamber and a low pressure in the LAPD ($P_{max} \sim 10^{-2}$ Pa) since it would require a large increase in the existing pumping speed of the vacuum system. Charge exchange of the helium beam ions with the neutrals imposes even more stricter limit on the maximum allowable neutral pressure in the ion source. Therefore, a pulsed injection of the neutral gas with a 1/3 Hz repetition rate is utilized to minimize the gas load. Three turbo-molecular pumps (one pump with a 3400 L/s and two pumps with 1000 L/s pumping speed) are mounted on the ion source chamber to maintain the high neutral-pressure gradient between the plasma chamber and the LAPD. The region between the turbo-molecular pumps is isolated using three vacuum baffles as shown in Fig. 1. Each vacuum baffle has a circular opening of 15.0 cm diameter to allow the passage of the ion beam.

The RF source is triggered to generate the plasma immediately after sufficient neutral pressure has built up in the ceramic dome. Excess neutrals expand away from the ground grid forming a neutral gas cloud with an estimated axial expansion length of 2.5 m when the ion beam is turned on. A 23 keV helium ion beam takes about 2.5 μs to emerge from this neutral gas cloud. Charge exchange of the fast helium ions with the neutrals is a dominant loss mechanism which is much more severe in the neutral gas cloud than in the LAPD. In the beam-plasma experiments, a 2.0×10^{-3} Pa (1.5×10^{-5} Torr) average helium pressure ($n_n = 5.3 \times 10^{17}$ m^{-3}) is maintained in the LAPD. The charge exchange cross section σ_{cex} (Ref. 26) for a 15–25 keV helium ion beam is $\sim 5 \times 10^{-20}$ m^2. Thus, the charge exchange mean-free-path [$\lambda_{cex} = 1/(n_n \sigma_{cex})$] for the ion beam in the LAPD plasma is ∼38 m. This is larger than the length of the LAPD plasma (∼17 m), therefore, no significant loss of the beam ions is expected once it emerges from the neutral gas cloud and enters the magnetized plasma of the LAPD.

A comparison of the ion beam profiles in the ion source chamber and in the LAPD plasma evince that ∼25% of the ion beam particles are lost in the neutral gas cloud. This measurement also indicates that the average neutral pressure in the neutral gas cloud is $\sim 10^{-2}$ Pa. Operating the ion source below the ceramic dome pressure mentioned above made it extremely difficult to produce a stable RF plasma in the ion

source. Note that the ion beam travels a 4.3 m axial distance before entering the magnetized plasma of the LAPD. In this 4.3 m beam-path, it travels through the neutral gas cloud and also the region of the LAPD plasma outside its end magnetic coils. In this exterior region, magnetic field lines of the LAPD flare out forming a strong radial component. The beam loss due to these diverging magnetic field lines is minimized by maintaining a low beam divergence.

D. Grid safety and control system

The ion source has been designed for an unattended operation which is critical for acquiring the data during computer-controlled experiments on the LAPD. Such experiments are often performed overnight and require several hours to complete. A reliable control system has been built for this purpose. The control system safely turns off the high-voltage pulser, RF plasma source, and the gas injector valve in the event of the fault conditions. Typical fault conditions are a high-pressure buildup in the ion source, arcs with more than 15 A current transients (both internal and external to the extraction system), no plasma in the ceramic dome, and an extended power outage. A leakage in the vacuum system, malfunctioning of the pumps, and failure of the gas injector valve are the main reasons for the high-pressure fault. The thermal overload on the grid is not an issue during normal operation of the LAPD ion source, since the average beam power in the pulsed injection of the LAPD ion beam is only 10 W. However, a big arc between the grids or a continuous arcing between the grids due to fault conditions (e.g., failure of the gas injector valve) have the potential to damage the grids by sputtering or sudden buildup of the heat load. Therefore, such arcs must be prevented.

The main component of the control system is an arc-fault detector. The arc-fault detector circuit has been developed to prevent the frequent occurrence of arcs that can damage the ion source grids or other equipment. A displacement current spike of several ampere magnitude is observed during the fast rise time ($\tau_{rise} < 4\ \mu$s) of the screen-grid voltage pulse. This displacement current spike is caused by the 360 pF stray capacitance between the system ground and the screen grid. This current spike should not generate a fault condition. A stray capacitance neutralization circuit (see Fig. 3(b)) has been developed to remove this displacement current spike from the fault-current monitoring system. A compensating capacitor is tuned in the circuit to remove the spike from the compensated output signal. The waveform of the actual arcs is found to be quite different from the displacement current spike. Therefore, the current due to the arcs is not compensated by the circuit shown in Fig. 3(b) and an arc fault condition is generated.

A comparator circuit generates the arc fault condition if the compensated current exceeds the set threshold (~15 A). Following the detection of the arcs, the accelerating voltage is disabled for a period of typically one second. This permits the continuous operation of the ion source during the conditioning of the ion source grids. On continuous generation of the arc fault conditions, a counter generates a continuous-arc fault condition and turns off all the power supplies and the RF source for a manual reset. On detection of the high-pressure faults, a gate-valve separating the ion source and the LAPD is closed to protect the LAPD cathode.

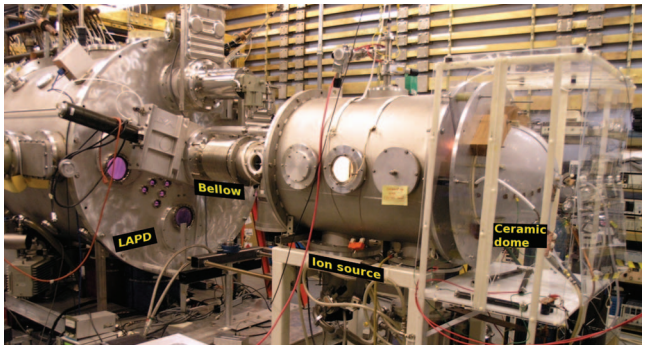

FIG. 4. (Color online) Photograph showing the ion source mounted at the end of the LAPD. Only a small portion of the LAPD is seen in this photograph. The flexible bellow is placed between the ion source chamber and the LAPD. The ion source chamber is mounted on wheels and can be rotated around the pivot located in the middle of the bellow.

V. RESULTS AND DISCUSSION

A picture of the ion source setup on the LAPD is shown in Fig. 4. The ion source is mounted on wheels and connected to the LAPD end by a rotatable frame resting on a heavy-duty ball-bearing. The ball-bearing is mounted to the LAPD end-flange and placed under the flexible bellow to form the pivot for the rotation in the horizontal plane. This arrangement facilitates the oblique beam injection in a $\pm 15^\circ$ angular range with a 0.5° precision.

Measurement of the ion-saturation current-density J using a disk-shaped Langmuir probe (area: 1.5×10^{-5} m^2) in the plasma chamber is presented in Fig. 5. The probe was biased at -90 V to collect the ion saturation current and placed on the discharge axis at a 1.5 cm distance from the screen grid. The observed linear increase in J (without an abrupt change) with the input RF power is favorable since it helps in ensuring the controlled variation of the beam current [$j_b \propto V_0^{3/2}$ in accordance with Eq. (4)] during variable beam-voltage operations. These measurements also demonstrate that the 28 kW RF source can produce a sufficiently dense plasma ($n \sim 10^{19}$ m^{-3}, $T_e \sim 7$ eV) which is more than adequate for our requirements. A fairly uniform plasma ($\partial J/|J| < 0.02$) across the surface area of the screen grid was obtained in the ICP source. Results for a 23 kV helium ion beam are discussed in the following paragraphs.

In a stand-alone operation, the ion source was tested up to 23 kV with 3.7 A optimal beam current to generate a least divergent beam (~1.0°). In order to obtain a minimum divergence of a 23 kV helium ion beam, a 4.1 A beam current should be extracted using our extractor system according to Eq. (4). Considering the fact that this theoretical estimate is based on the existence of the ideal beam extraction conditions as outlined in Sec. III, the result shows a reasonably good agreement with the theory.

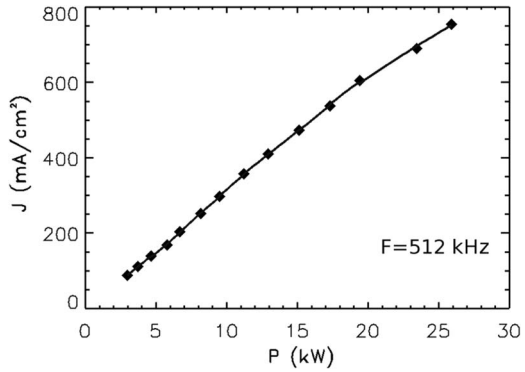

FIG. 5. Dependence of the ion-saturation current-density J on the input RF power in the ceramic dome plasma.

After integration of the ion source to the LAPD, the source was operated at a lower beam current (2.0 A instead of 3.7 A at 23 kV). This served to keep the neutral gas pressure in the beam path below an acceptable limit. The higher neutral pressure was undesirable since a large fraction of the ion beam was converted to a neutral beam at a higher pressure making it unsuitable for the LAPD fast ion experiments. To compensate for the increase of the beam divergence due to operation of the source at a lower beam current, two magnetic focusing coils ($B_{max} \sim 800$ G) were used in the beam path (see schematic in Fig. 1) and finally a low divergence ion beam ($\sim 0.8^{\circ}$) was injected in the LAPD plasma. Figure 6 shows the beam profile for a 23 kV/2.0 A ion beam at 1.5 ms in the afterglow of the ambient plasma measured using a fast ion collector (see Sec. IV B). The ion beam was injected axially in the LAPD and the measurement was performed at a 11.09 m distance from the ground grid. The FWHM of the ion beam at this location is 8 cm – same as the width of the ion source grids.

The profile measurement for a 23 kV/2.0 A ion beam in Fig. 6 implies that 9.0×10^{14} m^{-3} maximum ion beam density [$n_b = j/(ev_b)$] was achieved in the afterglow of the LAPD plasma. Similar results for the maximum current density j and n_b are obtained by injecting the beam in the main plasma. Thus, ratio of the beam pressure and the plasma pressure β_b/β_p is 2.1 in the main plasma ($n = 2.0 \times 10^{18}$ m^{-3}, $T_e \sim 5.0$ eV) and it is 41.4 in the afterglow plasma ($n \sim 10^{18}$ m^{-3}, $T_e \sim 0.5$ eV). This indicates that a significant pressure perturbation is caused by the ion beam in the plasma. Figure 7 shows a typical fast-ion collector signal in the LAPD plasma. The signal was recorded in the central (yellow online) beam-spot region of Fig. 6. The time-of-flight of the ion beam pulse implies a $\sim 1.01 \times 10^6$ m/s axial velocity – comparable to the injected axial velocity of the ion beam ($v_b \sim 1.05 \times 10^6$ m/s).

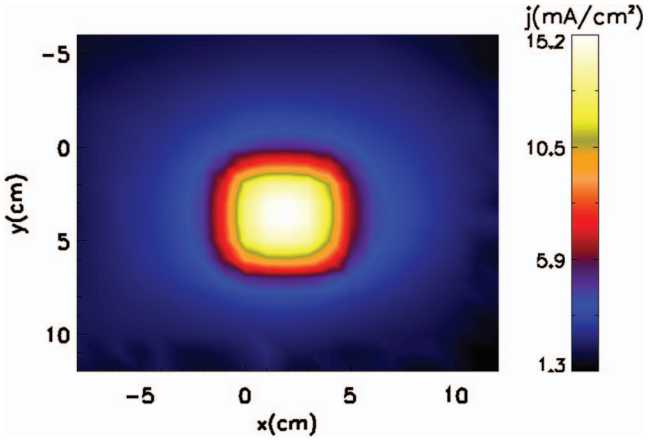

FIG. 6. (Color online) Ion beam profile in the LAPD plasma, measured at a 11.09 m axial distance from the ground grid.

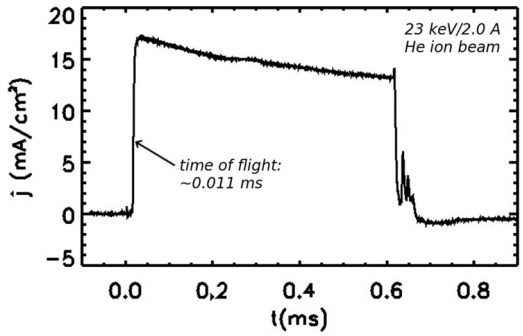

FIG. 7. Time evolution of the ion beam current density j in the LAPD plasma. The beam current density was measured at a 11.09 m axial distance from the ground grid

The results presented in this section demonstrate that the LAPD ion source fulfills the design goals described in Sec. II. The fast-rise time of the beam pulse, its undistorted shape after traveling several meters in the plasma, and observation of a tight beam-spot at multiple axial locations manifest that the LAPD ion source can produce a good quality, low divergence ion beam for fusion relevant fast-ion experiments.

ACKNOWLEDGMENTS

The authors thank Z. Lucky, M. Drandell, and M. Nakamoto for their expert technical assistance and gratefully acknowledge valuable discussions with T. N. Stevenson, L. Grisham, and W. W. Heidbrink. The research was jointly supported by US DOE and NSF for a fusion research campaign at the Basic Plasma Science Facility, UCLA.

[1] H. R. Kaufman, J. J. Cuomo, and J. M. E. Harper, J. Vac. Sci. Technol. **21**, 725 (1982).
[2] J. M. E. Harper, J. J. Cuomo, and H. R. Kaufman, J. Vac. Sci. Technol. **21**, 737 (1982).
[3] U. Fantz, P. Franzen, W. Kraus, M. Berger, S. Christ-Koch, M. Frschle, R. Gutser, B. Heinemann, C. Martens, P. McNeely, R. Riedl, E. Speth, and D. Wnderlich, Plasma Phys. Controlled Fusion **49**, B563 (2007).
[4] Y. Okumura, Y. Fujiwara, M. Kashiwagi, T. Kitagawa, K. Miyamoto, T. Morishita, M. Hanada, T. Takayanagi, M. Taniguchi, and K. Watanabe, Rev. Sci. Instrum. **71**, 1219 (2000).
[5] M. M. Menon, C. C. Tsai, J. H. Whealton, D. E. Schechter, G. C. Barber, S. K. Combs, W. K. Dagenhart, W. L. Gardner, H. H. Haselton, N. S. Ponte, P. M. Ryan, W. L. Stirling, and R. E. Wright, Rev. Sci. Instrum. **56**, 242 (1985).
[6] D. Schardt, T. Elsässer, and D. Schulz-Ertner, Rev. Mod. Phys. **82**, 383 (2010).
[7] *The Physics and Technology of Ion Sources*, 2nd ed., edited by I. G. Brown (Wiley-VCH, Berlin, 2004).
[8] R. S. Houk, V. A. Fassel, G. D. Flesch, H. J. Svec, A. L. Gray, and C. E. Taylor, Anal. Chem. **52**, 2283 (1980).

[9]W. Gekelman, H. Pfister, Z. Lucky, J. Bamber, D. Leneman, and J. Maggs, Rev. Sci. Instrum. **62**, 2875 (1991).
[10]D. Leneman, W. Gekelman, and J. Maggs, Rev. Sci. Instrum. **77**, 015108 (2006).
[11]W. Gekelman, S. Vincena, B. V. Compernolle, G. J. Morales, J. E. Maggs, P. Pribyl, and T. A. Carter, Phys. Plasmas **18**, 055501 (2011).
[12]H. Alfvén, Nature (London) **150**, 405 (1942).
[13]G. J. Morales, R. S. Loritsch, and J. E. Maggs, Phys. Plasmas **1**, 3765 (1994).
[14]G. J. Morales and J. E. Maggs, Phys. Plasmas **4**, 4118 (1997).
[15]K.-L. Wong, Plasma Phys. Controlled Fusion **41**, R1 (1999).
[16]W. W. Heidbrink, Phys. Plasmas **15**, 055501 (2008).
[17]Y. M. Li, S. M. Mahajan, and D. W. Ross, Phys. Fluids **30**, 1466 (1987).
[18]J. Kim, J. H. Whealton, and G. Schilling, J. Appl. Phys. **49**, 517 (1978).
[19]J. R. Coupland, T. S. Green, D. P. Hammond, and A. C. Riviere, Rev. Sci. Instrum. **44**, 1258 (1973).
[20]M. A. Ray, S. A. Barnett, and J. E. Greene, J. Vac. Sci. Technol. A **7**, 125 (1989).
[21]J. Hopwood, Plasma Sources Sci. Technol. **1**, 109 (1992).
[22]P. Pribyl, U.S. patent 7,084,832 (1 August 2006).
[23]H. Goede, J. M. Dawson, and K. R. MacKenzie, Phys. Rev. Lett. **44**, 1066 (1980).
[24]J. Simpson, Rev. Sci. Instrum. **32**, 1283 (1961).
[25]Y. Yuan, J. Bansky, J. Engemann, and A. Brockhaus, Surf. Coat. Technol. **74–75**, 534 (1995).
[26]C. F. Barnett and P. M. Stier, Phys. Rev. **109**, 385 (1958).